Inorganic Chemistry

Article

pubs.acs.org/IC

A Dissociative Quantum Mechanical/Molecular Mechanical Molecular Dynamics Simulation and Infrared Experiments Reveal Characteristics of the Strongly Hydrolytic Arsenic(III)

Lorenz R. Canaval,[†] Oliver M. D. Lutz,[‡] Alexander K. H. Weiss,[†] Christian W. Huck,[‡] and Thomas S. Hofer*[,†]

[†]Theoretical Chemistry Division, Institute of General, Inorganic and Theoretical Chemistry, University of Innsbruck, Innrain 80-82, A-6020 Innsbruck, Austria

[‡]Institute for Analytical Chemistry and Radiochemistry, University of Innsbruck, Innrain 80-82, A-6020 Innsbruck, Austria

Supporting Information

ABSTRACT: This work presents a hybrid ab initio quantum mechanical/molecular mechanical simulation at the RI-MP2 level of theory investigating the hydrolysis process of arsenic(III), ultimately leading to arsenous acid (H_3AsO_3). A newly implemented dissociative water model has been applied to treat the interactions in the classical region, which is capable of describing non-neutral water species such as hydroxide and oxonium ions. Three stages of hydrolysis have been observed during the simulation and besides profound dynamical considerations, detailed insights into structural changes and atomic partial charge shifts are presented. In particular, the geometrical properties of H-bonds involved in each of the three proton transfer events and subsequent proton hopping reactions are discussed. A Laguerre tessellation analysis has been employed to estimate the molecular volume of H_3AsO_3. Estimations of pK_a values of the arsenic(III)-aquo-complexes have been obtained at the G4 and CBS-Q//B3 levels of theory using a thermodynamic cycle, whereas rate constants for the final hydrolysis step have been determined via reaction path optimization and transition state theory. Newly recorded Fourier transform infrared (FT-IR) spectroscopy measurements have been compared to power spectra obtained from the simulation data, confirming its quality. The simulation findings, as well as results from computational spectroscopic calculations utilizing the PT2-VSCF methodology, proved valuable for the interpretation of the experimental FT-IR data, elucidating the particularities of the strongly observed IR Raman noncoincidence effect.

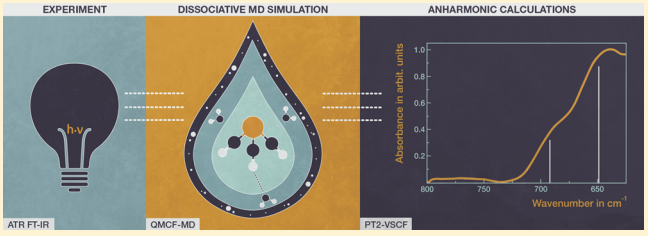

1. INTRODUCTION

Arsenic is potentially toxic to humans and classified a high priority issue by the World Health Organization.[1] It is released to the environment by both natural phenomena such as weathering, biological and volcanic activity, and anthropogenic processes.[2] The distribution of arsenic compounds is mainly controlled by dissolution of minerals and ores in water, industrial effluents, and dry dust fallout from the atmosphere.[1−3] A recent paper describes the mechanisms underlying the surface binding of arsenic(III) species to manganese oxide-coated-alumina, facilitating drinking water regeneration.[4] A very recent work on molecular adducts of aqueous arsenous acid and platinum(II) reports cellular cytotoxicity and biological activity in several cancer cell lines,[5] further emphasizing the strong interest in the behavior of As(III) in an aqueous environment.

Because of the far reaching interest in aqueous arsenic species, it seemed promising to conduct a hybrid quantum mechanical/molecular mechanical (QM/MM) simulation and a series of experimental measurements. Since As(III) compounds such as $AsCl_3$ are known to be sensitive to moisture, yielding products of hydrolysis, it was of supreme importance to combine the quantum mechanical charge field molecular dynamics (QMCF-MD) approach with a dissociative water model,[6,7] properly describing protonated and deprotonated water molecules beyond the quantum mechanically treated region. Up to the present day, QM/MM hybrid simulations had to be aborted as soon as oxonium or hydroxide ions left the quantum mechanically treated region[8−10] because of the inability of classical potentials to adequately describe these species, including proton transfer (PT) events. The dissociative water model enables an adequate treatment of these phenomena in the MM region of a QM/MM setup, offering a number of new opportunities when investigating hydrolyzing systems such as As(III), Ge(IV), or Pb(IV). Obviously, studies modeling acidic or basic aqueous environments may now also be conducted. Herein, we present a study of the strongly Lewis-acidic arsenic(III), reacting via three hydrolysis processes to the final product of fully protonated arsenous acid (H_3AsO_3). While three hydroxide ions remain bound to the ion, being part of the nearly C_{3v} symmetric arsenous acid, three oxonium ions,

Received: January 7, 2014
Published: August 26, 2014

   dx.doi.org/10.1021/ic4031156 | Inorg. Chem. 2014, 53, 11861−11870

formed as a result of the hydrolysis, may freely migrate between QM and MM region.

Complementing the simulation, we report theoretically derived infrared (IR) spectra calculated via the well-established PT2-VSCF approach. These calculations have been conducted to study the influence of the basis set on the accuracy of the spectroscopic results. This procedure helped to find an optimal compromise between accuracy and computational feasibility for the highly demanding QMCF-MD simulation, which was carried out employing the resolution-of-identity Møller−Plesset second order perturbation theory (RI-MP2), accounting for electron correlation. As only Raman spectra of aqueous arsenous acid were found in the literature, FT-IR spectra of solutions known to exclusively contain H_3AsO_3 were directly compared to the theoretical predictions. Interestingly, a significant IR Raman noncoincidence effect was observed, which has already been reported for a number of molecular liquids,[11,12] however not for protonated As_2O_3. In this context, the importance of computational investigations is shown to facilitate explanations for experimental observations such as the IR Raman noncoincidence effect.

2. COMPUTATIONAL AND EXPERIMENTAL SETUP

2.1. Simulation Methodology. The QMCF-MD ansatz[13,14] is based on the hybrid QM/MM MD approach,[15−17] dividing the system into QM and MM subregions. A number of methodological improvements over conventional QM/MM techniques characterize the QMCF-MD ansatz. The enlarged quantum mechanically treated region is further split into a core and a layer zone, enabling the neglect of non-Coulombic interaction potentials between species in the MM zone and particles located in the QM core zone. This is a great benefit as the design of such potentials is often very difficult and time-consuming. Furthermore, an electrostatic embedding of the QM zone is realized by taking the atomic point charges of all atoms in the MM region into account, which ensures a bulk-like environment avoiding artifacts resulting from an artificial in vacuo treatment of the QM zone. Additionally, quantum mechanically derived partial charges are used to evaluate the Coulombic interactions of atoms being part of the QM zone. As the forces acting upon particles migrating between the QM and the MM region have to be continuous, a smoothing technique gradually adjusting the forces from the QM to the MM contribution has been developed. Further details on the methodology are described elsewhere.[13,14,18,19]

While no problems arise when chemical reactions such as PT reactions take place within the quantum mechanically treated region, bond formation and cleavage in the MM region must be carefully parametrized. In particular, a suitable treatment of oxonium and hydroxide ions and associated PT phenomena by classical means is a very challenging task.[20−29] However, the dissociative water model developed by Mahadevan and Garofalini[7] provides a suitable approach enabling an adequate description of such species and reactions. The interatomic potential consists of both pair and screened three-body contributions and employs the Wolf summation[30] to account for long-range Coulombic interactions. This water model proved to be compatible for implementation in a QM/MM setup and a procedure to master the technical challenges has recently been presented.[6] This includes an automated topology update which is necessary when aiming at a hybrid QM/MM approach rather than at a purely classical simulation technique as solvent molecules have to be assigned as a whole to either the QM or the MM zone. As the present study treats excess protons, the influence of nuclear quantum effects on PT reactions has to be assessed critically. While it has been shown that zero-point vibrations may indeed lower the reaction barrier,[31] tunneling effects were proven to have a low influence in transfer reactions of excess protons,[32−34] thus qualifying the aforementioned simulation setup as a realistic treatment.

2.2. Computational Spectroscopy Methods and the Choice of Basis Set. The significant computational effort involved in hybrid QM/MM-MD simulations, especially when involving ab initio methods explicitly including electron correlation, implies the usage of a computationally feasible basis set while preserving an accurate description of the system. In this study, the chosen basis set is justified by employing sophisticated anharmonically corrected frequency evaluations, going far beyond the qualities of the conventionally employed harmonic oscillator approximated (HOA) frequencies. In the vibrational self-consistent field (VSCF) approach,[35−39] the Hessian matrix is employed as a primary reference. Subsequently, point-wise displacements within the fundamental modes and their pairs are performed, yielding a complex potential energy surface of energies and dipoles for which Schrödinger's equation is solved numerically. The VSCF results may then be improved by means of higher corrective techniques such as second-order perturbation theory (i.e., PT2-VSCF).[40−42] For the case at hand, the geometry optimizations as well as the anharmonic corrections have been carried out with the GAMESS release dated May 1, 2012.[43] The PT2-VSCF evaluation of the PCM augmented[44] H_3AsO_3 molecule was initially carried out with Dunning's correlation-consistent triple-ζ basis set,[45] and the inner 10 electrons of arsenic were treated with the Stuttgart small-core ECP to reduce computational effort and to account for non-negligible relativistic effects of core electrons.[46] The resulting absorption band locations for the symmetric (ν_s, A_1) and the asymmetric (ν_{as}, E) mode of the As−O bond were computed as 692 and 649 cm^{-1}, respectively, which is in excellent agreement with the experimentally obtained values of 698 and 643 cm^{-1}. Subsequent benchmarks on the employed computational platform (12 2.93 GHz CPUs with 32 GB of RAM) have shown, however, that a QMCF-MD simulation at the RI-MP2 level of theory in conjunction with a triple-ζ basis set is currently beyond feasibility. Hence, the computationally less expensive and well-established 6-31G(d,p) basis set[47] for oxygen and hydrogen along with the cc-pVDZ-PP[46] basis set for arsenic have been investigated by means of a PT2-VSCF calculation, yielding 679 and 643 cm^{-1} for the two stretching fundamentals. The still very good agreement with the experimental values permits the conclusion that the double-ζ arrangement may be employed for the QMCF-MD simulation without a significant sacrifice of accuracy. Because of the use of the resolution-of-identity technique, the computational effort for MP2 is only approximately 4−5 times higher compared to simulations performed at hybrid DFT or ab initio Hartree−Fock level of theory.

2.3. Simulation Protocol. The simulation box including one As^{3+} cation and 1000 water molecules was shaped cubically with a side length of 31.2 Å resulting in a density of 0.997 g/cm^3. Since it can be expected that the heat of reaction of the hydrolysis process may lead to an increase of temperature, a thermostatisation at 298.15 K via the Berendsen weak coupling algorithm[48] with a relaxation time of 0.1 ps was employed to ensure that the successive PT events can be treated at the same thermal conditions. For the radii of the quantum mechanical core and layer zone, values of 0.01 and 5.7 Å were chosen, respectively. This enables a full quantum mechanical treatment of the arsenic ion, its ligands and the first hydration shell of the complex. As the distance between the arsenic ion and MM particles is 5.7 Å, only electrostatic interactions based on quantum mechanically derived atomic partial charges are considered. Non-Coulombic contributions between theses species are negligible, and thus no empirical As(III)−water and As(III)−oxonium potentials had to be developed. A smoothing zone of 0.2 Å between the QM layer and the MM region was applied to overcome discontinuities of forces. The atomic partial charges of all QM atoms have been determined via Mulliken[49,50] population analysis in every MD step. To integrate the equations of motion, the velocity-Verlet algorithm was employed using a time step of 0.2 fs. Long-range electrostatic interactions above 10.0 Å were treated with the Wolf Summation technique[30] as defined in the Garofalini model.[7] Periodic boundary conditions and the minimum image convention were applied to ensure a bulk-like environment. Figure 1 depicts the partitioning of the system into QM and MM regions and illustrates the molecular species treated within these areas. The setup chosen is based on the simulation protocols of earlier investigations on the hydrolysis

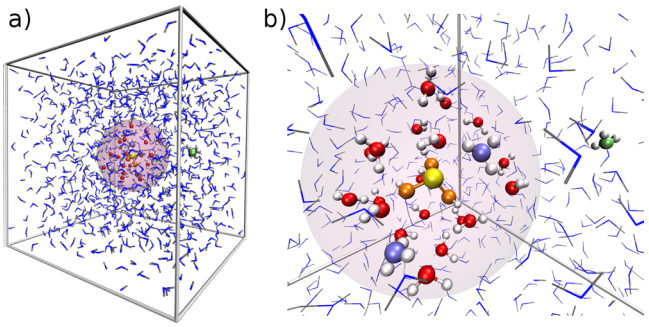

Figure 1. Snapshots obtained from the QMCF-MD simulation after three hydrolysis reactions illustrating (a) the partitioning of the system into a QM and a MM region and (b) giving a more detailed view into the QM zone. Two oxonium ions located inside the QM zone are colored blue, whereas the third oxonium ion being treated by the dissociative water potential in the MM region is illustrated in green. The H_3AsO_3 complex is highlighted in yellow–orange.

of As(III).[6,9,10] With arsenic(III)-potentials developed earlier,[9] a classical equilibration was conducted for 30 ps, which led to the starting configuration for the QMCF-MD simulation presented here. The initial total linear momentum was zero, which is a prerequisite when performing MD simulations. All QM calculations within that simulation were carried out with the TURBOMOLE 6.3 package[51−56] at the RI-MP2 level of theory. The trajectory has been visualized with the popular VMD package.[57]

2.4. Chemicals and Reagents. Arsenic(III) oxide (≥99.0%, Fluka AG, Buchs, Switzerland), perchloric acid (≥70%, Fisher Scientific Ltd., Leicestershire, United Kingdom), sodium hydroxide solution (≥50%, Sigma-Aldrich Chemical Co, Vienna, Austria), and water (LC-MS grade, Sigma-Aldrich Chemical Co., Vienna, Austria) have not been purified prior to the measurements. Saturated solutions of solid As_2O_3 in water have been prepared according to the procedure described by Loehr and Plane.[58] The solutions have been centrifuged for 2 min at 13000 rpm (centrifuge 5415 R, Eppendorf Austria GmbH, Vienna, Austria), and the supernatant was subsequently removed from the solid residuum in order to ensure absence of undissolved As_2O_3 in the liquid phase. In the same manner as described earlier,[58] a series of samples was produced, resembling final pH values ranging from 0 to 8, ensuring that H_3AsO_3 is the only arsenic containing species in solution.

2.5. Spectrometer Details. The samples were measured via attenuated total reflectance (ATR) Fourier transform (FT) mid-infrared (MIR) spectroscopy (Spectrum 100, PerkinElmer, Seer Green, United Kingdom) in the wavenumber region between and 600 cm^{-1}. It is worth mentioning that the manufacturer does not recommend utilization of the spectrometer's triglycine sulfate detector below 650 cm^{-1} due to an impaired signal-to-noise ratio (SNR) at high spectral resolutions. However, at a resolution of 4 cm^{-1}, the SNR in the region between 650 and 600 cm^{-1} was found to be on par with the domain > 650 cm^{-1}. Hence, the measurements have been carried out using a maximum interferometer retardation of 0.25 cm, reflecting a spectral resolution of 4 cm^{-1}. In every case, 20 scans were accumulated to gain a proper SNR, and strong Norton-Beer apodization[59] was employed. The spectrometer's calibration has been validated by employing the integrated methane cell at the resolution used during measurement of the samples.

Characterizing aqueous solutions via MIR spectroscopy is a challenging task due to the strong absorptions of water. Hence, and in order to obtain pure solute spectra, a solvent spectrum containing the respective amounts of $HClO_4$ and NaOH, respectively, was recorded as a background reference prior to each sample measurement. Because two fundamentals as well as lower lying deformation bands overlap strongly, the maxima in the experimental spectrum have to be investigated carefully. A 15-channel convolution was applied to each spectrum, and accurate absorption maxima were identified by fitting appropriate Gaussian functions to the curvature. Similarly, second derivative spectra with 10 symmetric side points provided a valuable alternative to obtain valid peak maxima.

3. RESULTS AND DISCUSSION

3.1. Data Obtained from the QMCF-MD Simulation. *3.1.1. Evolution of Structural Properties During the Hydrolysis Events.* A total of three hydrolysis steps induced by the strongly Lewis-acidic As^{3+} ion have been observed, ultimately yielding arsenous acid (H_3AsO_3) plus three excess protons forming oxonium ions in water. In this section, we will discuss the observed PT reactions in detail.

Figure 2a illustrates selected interatomic distances as a function of time for the first hydrolysis reaction observed after

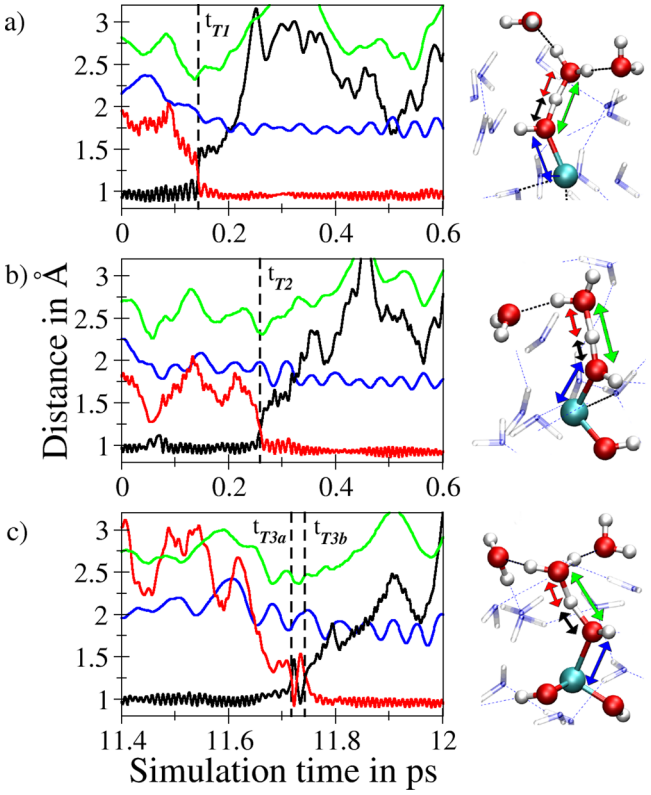

Figure 2. Selected interatomic distances characterizing (a) the first, (b) the second, and (c) the third hydrolysis reaction of As(III) for the corresponding transferring protons. Coloring of the arrows corresponds to that of the plots: donor–hydrogen (black), acceptor–hydrogen (red), donor–acceptor (green) and arsenic–donor (blue). Detailed figures for each hydrolysis step including analysis of neighboring water molecules of the acceptors species have been made available in the Supporting Information, Figures S1–3.

144 fs of the simulation (t_{T1}), resulting in a deprotonation of a water molecule coordinated to the As(III) ion. The transfer of this proton is indicated by a sharp increase of the donor–hydrogen distance, and a likewise decrease of the acceptor–hydrogen distance. In addition, a significant decrease of the donor–acceptor distance to 2.30 Å at the time of the PT is observed. Furthermore, the decrease of the arsenic–donor distance from 2.1 Å is starting even shortly before the PT occurs, leading to a final distance of approximately 1.75 Å, being in full agreement with experimental data for As–O distances in hydroxo-species.[60]

The influence of the geometries of H-bonds formed by two water molecules adjacent to the acceptor molecule (Figure

dx.doi.org/10.1021/ic4031156 | Inorg. Chem. 2014, 53, 11861−11870

S1b,c, Supporting Information) has been investigated. A strong hydrogen bond between the latter and a neighboring molecule was identified at the moment of the PT (t_{T1}, Figure S1b). A significant decrease of the corresponding donor−acceptor and acceptor−hydrogen distances to 2.74 and 1.77 Å, respectively, coupled with a near-linear arrangement of the acceptor−hydrogen−donor atoms (173°) highlights the cooperative influence of this H-bond during the reaction. In contrast, the second water molecule did not show any particular promoting influence. As both the arsenic-hydroxo-complex and the newly formed oxonium ion are positively charged, they tend to part, either by diffusion or by further proton hopping processes. Such a hopping event is observed 550 fs after the initial PT event (t_{H1}, Figure S1c).

A further interesting observation is the shortening of the donor−acceptor distances (r_{DA}) of the H-bonds associated with Figure S1a,b just prior to the PT event t_{T1}. A similar behavior has been observed in a simulation study of the PT from H_3O^+ to an adjacent H_2O using the Mahadevan-Garofalini potential, where a decrease of r_{DA} prior to the actual proton-transfer was reported too.[61] Since the simultaneous alignment of hydrogen bonds at the same water molecule is in general known to have a synergistic effect, it can be concluded that the near-perfect arrangement of a neighboring H-bond promotes a favorable alignment of the donor-hydrogen-acceptor bond involved in the PT. The shortening of the donor−acceptor distance leads to a decrease of the potential energy, which enables the transferring proton to build up a sufficient momentum to overcome the potential energy barrier arising from the subsequent increase of r_{DA}.

In order to investigate this hypothesis, the velocity component parallel to the donor−acceptor distance was compared with the total amount of the velocity of the transferring proton after elimination of the joint center-of-mass momentum of the donor-hydrogen-acceptor system (Figure 3). As can be seen, the parallel velocity component $v^{\parallel}$ of the proton is in general noticeably smaller than its total velocity v except during the proton-transfer, where they nearly coincide, effectively eliminating all velocity components perpendicular to the donor−acceptor vector. A further notable feature visible for both depicted velocities is the intermediate minimum exactly at the time the proton-transfer takes place (t_{T1}). This decrease of the velocity clearly demonstrates that the proton has to overcome a slight potential energy barrier along the reaction coordinate. It can be further seen from Figure 3 that although during some instances the total velocity of the proton is even higher than during the PT event, the respective parallel component is significantly smaller. Only one other instance of a sufficiently high parallel velocity occurring at about 0.1 ps is visible; however, the associated donor−acceptor distance is approximately 2.75 Å and therefore the potential energy barrier along the reaction path can be expected to be much higher. From this analysis, it can be concluded that a cooperative effect of different H-bonds, the shortening of the donor−acceptor distance along with the channeling of the proton velocity parallel to the donor−acceptor distance promoted the occurrence of this particular PT.

Figure 2b depicts the second hydrolysis of a water molecule bound to the ion (t_{T2}) after a simulation time of 259 fs, induced by the still strongly Lewis-acidic $[As(OH)]^{2+}$ complex. Similar to the first event, this PT reaction is characterized by a sharp inversion of the donor−hydrogen and the acceptor−hydrogen distance together with a minimum donor−acceptor distance of

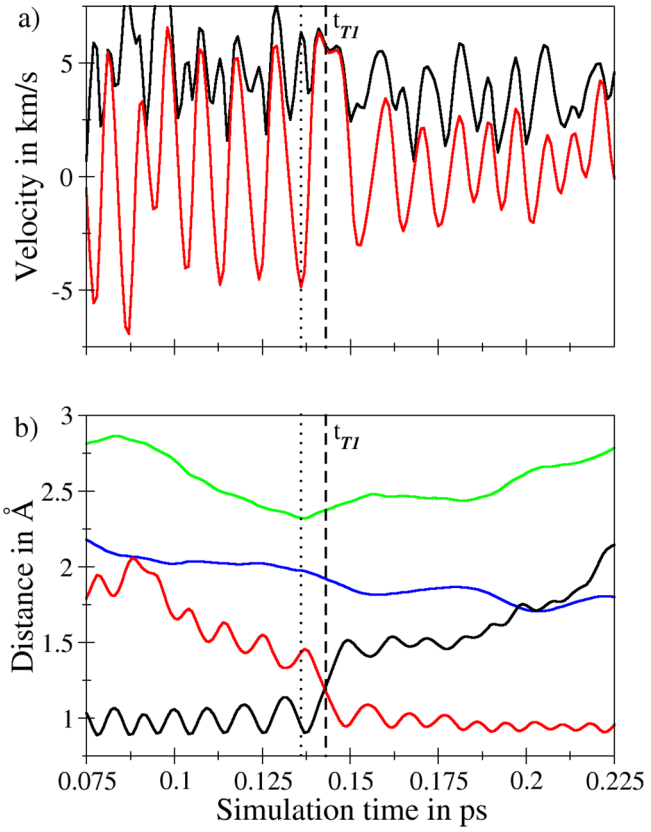

Figure 3. Detailed analysis of the first PT event: (a) total velocity v of the transferred proton (black) and the corresponding parallel component $v^{\parallel}$ (red), and (b) enlarged view of selected interatomic distances as shown in Figure 2a (coloring: donor−hydrogen: black, acceptor−hydrogen: red, donor−acceptor: green and arsenic−donor: blue).

2.30 Å. Again a neighboring water molecule promotes the PT (Figure S2b) via a cooperative H-bonding to the H−acceptor molecule. The corresponding acceptor−hydrogen distance amounts to 1.44 Å, the acceptor−donor distance is 2.40 Å, and the H-bond angle is found to be 172°. Analogous to the first hydrolysis process, a subsequent proton hopping reaction is observed 100 fs after the PT event induced by $[As(OH)]^{2+}$.

In contrast to the first two hydrolysis events taking place very soon, a number of hydrolysis attempts were observed during 10 ps before the third successful PT reaction occurred after approximately 12 ps of simulation time (t_{T3b}, Figure 2c). An unsuccessful PT event was noticed 25 fs earlier (t_{T3a}, Figure 2c). The respective distance plots do not reveal any significant differences between these two events in terms of stabilization via H-bonding by the two neighboring water molecules (Figures S3b,c). However, the analysis of the corresponding H-bond angles reveals that during the first transfer attempt (t_{T3a}) only one H-bond shows an angle close to 180°, whereas the second one corresponds to a weak H-bond, amounting to 138° only. In contrast, both H-bond angles show values close to linearity for the successful attempt (t_{T3b}, Figure S3d). It can be concluded that this near perfect alignment rigidly stabilizes the acceptor molecule, thus promoting the final hydrolysis step, resulting in arsenous acid. Detailed characteristics of the H-bonds involved in the three hydrolysis steps are presented in Table 1. It is important to note that only two water molecules acting as H-bond acceptors are participating in the third PT

dx.doi.org/10.1021/ic4031156 | Inorg. Chem. 2014, 53, 11861−11870

Table 1. Characteristics of H-Bonds Involved in the Hydrolytic Conversion of As(III) in Aqueous Environment during the QMCF-MD Simulation: Acceptor−Proton Distance in Å (d_{A-H}), Acceptor−Donor Distance in Å (d_{A-D}) and Acceptor−Proton−Donor Angle (a_{A-H-D}) in Degree

description	d_{A-H}	d_{A-D}	a_{A-H-D}
first PT (0.14 ps)	1.77	2.74	173
second PT (0.26 ps)	1.63	2.50	150
third PT, first attempt (11.72 ps)	1.66	2.68	178
	1.85	2.68	138
third PT, second attempt (11.74 ps)	1.63	2.59	170
	1.73	2.65	170

event, while the presence of further water molecules acting as H-bond donors as reported in studies of the proton transport mechanism in bulk has not been observed.[62,63]

The results found, especially the rapidity of the first two hydrolysis reactions, are in very good agreement with earlier attempts to investigate the As(III) reactivity in water. Bhattacharjee et al. employed the Hartree−Fock (HF) level of theory in a QMCF-MD simulation and reported two PT reactions after 0.18 and 0.27 ps.[9] A first simple test run of the dissociative water model in conjunction with the QMCF-MD framework employing also HF, revealed hydrolysis events after 0.21 and 0.56 ps.[6] In contrast to our simulation conducted at the RI-MP2 level of theory, the aforementioned simulations did not show a third hydrolysis reaction, although they exhibited a longer simulation time (15 and 20 ps). This emphasizes the essential role of correlation effects to adequately describe the hydrolytic center plus its hydration environment. A Car-Parrinello MD study performed by Coskuner et al. yielded the first hydrolysis reaction of As(III) in water after 60 fs simulation time, which is in reasonable agreement with our finding.[64]

3.1.2. Evolution of Partial Charges During the Hydrolysis Events. In addition to structural properties, quantum mechanically derived partial charges have been analyzed to investigate charge−transfer effects initiating and following the three hydrolysis events. Figure 4a,d depicts the evolution of selected partial charges of As for two different time intervals. Because of charge−transfer effects, which are intrinsically accounted for in the quantum mechanical treatment, the formal charge of As(III) is reduced to +2.0 a.u. at the beginning of the simulation. As can be seen in plot 4a, the partial charge of the ion drops to +1.85 a.u. before the first PT event takes place, and then a short stagnation at this level lasting about 80 fs is observed. During this time the first successful hydrolysis event takes place (t_{T1}). Subsequent continuous discharging of the center ion is observed, leading to a value of about +1.70 a.u., where again short stagnation and the second successful hydrolysis event occurs (t_{T2}). After this event, shift of electron density to the ion is still observed, resulting in a minimum partial charge of +1.45 a.u, which rises to +1.55 within 50 fs. A final charge−transfer initiating and following the third PT event (t_{T3b}) leads to a minimum charge of +1.20 a.u for As, rising to a final value of +1.35 a.u. within about 200 fs. The arsenic ion (Figure 4a) and the oxygen atom of the coordinated water molecule (Figure 4b, blue) receive electron density before the first PT reaction occurs at t_{T1}. The partial charge of As drops from +2.05 to +1.85 au, that of the oxygen atom from −0.80 to −1.00 au. In contrast, the atoms of the newly formed oxonium ion are continuously donating electron density. The acceptor oxygen (Figure 4b, red) experiences a change from −0.90 to

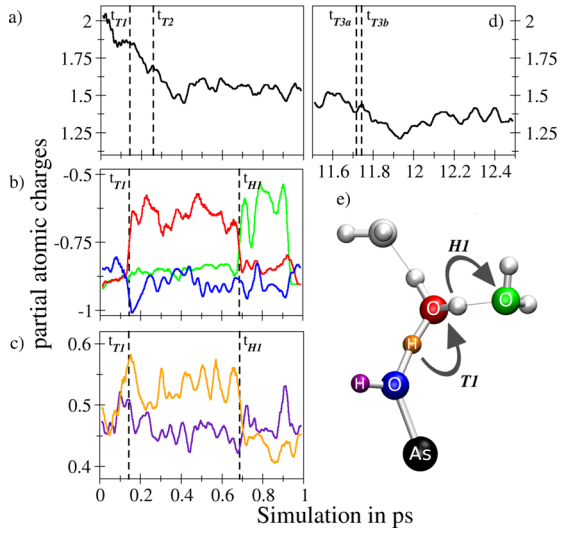

Figure 4. Evolution of quantum mechanically derived partial charges (running averages with a length of average of 25 fs) for selected atoms (first and second hydrolysis event including subsequent H-hopping: (a) arsenic, (b) oxygens, (c) hydrogens, and third hydrolysis: (d) arsenic). The colors of atoms in illustration (e) correspond to those in the plots.

−0.60 au, the transferred proton (Figure 4c, orange) an increase of the partial charge from +0.50 to +0.60 au. An equilibration of partial charge of the hydroxo-oxygen (Figure 4b, blue) at −0.90 a.u. is observed after the successful PT event.

At t_{H1} (Figure 4b,c), a proton hopping process is detected via monitoring the partial charges of the atoms involved. The plot is characterized by a likewise inversion of the oxygens' partial charges from −0.85 to −0.60 a.u. and vice versa.

Figure 4c shows the evolution of partial charges of the two hydrogen atoms initially bound to the water molecule coordinated to As(III). The same trend, namely, a rise from +0.45 to +0.52 au, is observed for both atoms for the first 100 fs of simulation time. After that, a significant differentiation takes place, with the charge of the transferring proton increasing close to +0.60 au, while the other one drops to its initial value, the corresponding atom remaining part of the newly formed hydroxo-species. Since quantum mechanically derived partial charges show pronounced variations upon PT events, they are a versatile tool to monitor such reactions in QM simulations.

3.1.3. Characterization of H_3AsO_3 from the Simulation Data. Arsenous acid, H_3AsO_3, the product formed after three hydrolysis events, has been characterized via a number of structural and dynamical methods (Figure 5). The peak maxima in the As−O RDF were found at 1.80 and 3.60 Å, which can be attributed to the three hydroxyl groups and the first hydration shell surrounding the acid, respectively. The first value is in excellent agreement with data reported in the literature for 3-fold coordinated As(III) species.[60] An As−O distance of 1.76 Å was reported for a CP-MD simulation of As^{3+} in water.[64] Analysis of the O−As−O angle via an angular distribution function (ADF) yielded a distinct maximum at 95°. A Laguerre tessellation analysis,[65,66] resembling the weighted variant of the Voronoi decomposition,[67] is employed to study the molecular volume of H_3AsO_3. The atomic radii for arsenic(III), oxygen, and hydrogen have been chosen as 58,[68] 152,[69] and 110 pm,[69] respectively. Finally, the average molecular volume of arsenous acid was calculated to be 75 ± 10 Å^3.

dx.doi.org/10.1021/ic4031156 | Inorg. Chem. 2014, 53, 11861−11870

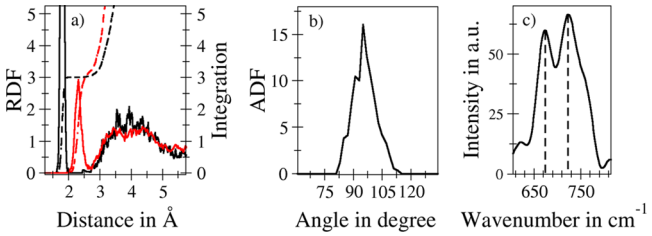

Figure 5. Characteristics of arsenous acid H_3AsO_3 obtained from the simulation data: (a) As−O (black) and As−H (red) radial distribution functions including their running integration information, (b) O−As−O angular distribution function, and (c) power spectrum calculated via velocity autocorrelation functions and subsequent Fourier transformation.

Power spectra from the simulation data were obtained via Fourier transformed velocity autocorrelation functions (VACFs), characterizing the strength of the arsenic−oxygen bond. Using a sampling time of 1.5 ps, two peak maxima were identified at 723 and 674 cm^{-1}, being attributed to ν_s (A_1) and ν_{as} (E), respectively. Given the fact that the wavenumbers of the underlying fundamentals depend on the second derivatives of the energy with respect to the nuclear coordinates, they are considered a very sensitive probe of the simulation's accuracy. The mean deviations from previously reported Raman spectra[3,58,70] and the newly recorded FT-IR data (Table 2) are <2.4% and <4.2%, respectively, both confirming the simulation's quality. Because such data does not resemble actual fundamental excitations as observed in an IR experiment ($\Delta\nu$ = 1) but rather oscillations about the vibrational ground state, the intensities obtained from VACF derived power spectra may not be compared to either IR or Raman data.

Table 2. Comparison of Experimentally Found FT-IR Absorption Maxima and Raman Shifts with Computationally Derived Results at the MP2/PT2-VSCF/cc-pVTZ Level of Theory and Values Obtained from the QMCF-MD Simulation Obtained via Fourier Transformed VACFs[a]

mode	ATR FT-IR	Raman[3,58,70]	PT2-VSCF	QMCF-MD
ν_s (A_1)	698	710	692	723
ν_{as} (E)	643	655	649	674

[a]All values are given in cm^{-1}.

3.2. FT-IR Characterization of Aqueous H_3AsO_3. The characteristics of hydrated arsenous acid have been studied in the past via Raman spectroscopy.[3,58,70] In 1958, Loehr and Plane presented Raman spectra of arsenous acid and other arsenite species in aqueous environment.[58] From their data, they indicated that the equilibrium structure of the fully protonated acid may either belong to the D_{3h} or the C_{3v} point group but given the location of the two Raman bands, they concluded C_{3v} symmetry, being in agreement with our simulation and the results from the geometry optimizations. The authors have assigned the two main bands at 710 and 655 cm^{-1} to ν_s (A_1) and ν_{as} (E) of the arsenic−oxygen bond, respectively. These values have been confirmed by Pokrovski et al. in 1996[3] and by Wood et al. in 2002.[70] Loehr and Plane found that H_3AsO_3 is stable in solutions with pH values ranging from 0 to ∼8.5, and they were able to provide strong evidence that aqueous arsenic(III) species are not liable to polymerization reactions, remaining stable in their monomeric form.[58]

Since to the best of our knowledge, no FT-IR spectrum of aqueous H_3AsO_3 has been reported to date, it seemed promising to investigate the species via this technique. The previously prepared samples (see Computational and Experimental Setup) of H_3AsO_3 were measured via ATR FT-IR spectroscopy and ν_s (A_1) and ν_{as} (E) of the As−O bond were identified at 698 and 643 cm^{-1}, respectively (Figure 6). It is

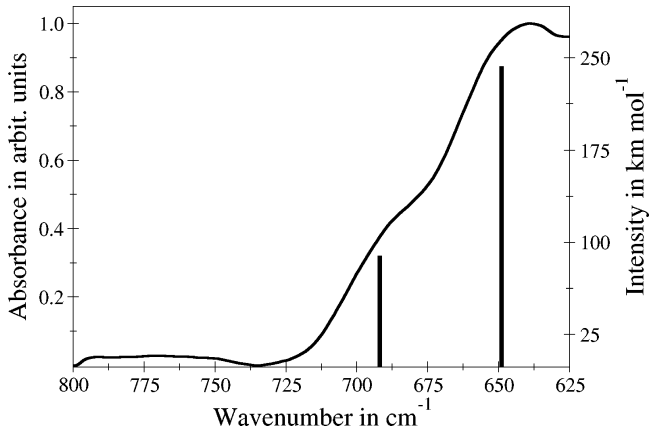

Figure 6. Exemplary FT-IR spectrum of aqueous H_3AsO_3 at pH 7 (left *y*-axis) compared to the data obtained via the PT2-VSCF approach (vertical bars, right *y*-axis).

worth mentioning that for all investigated solutions ranging from pH 0 to 8, identical locations of the absorption maxima have been observed, coinciding with the aforementioned findings by Loehr and Plane.[58] When compared to the Raman bands at 710 and 655 cm^{-1}, a significant red-shift of the FT-IR bands becomes evident, which is attributed to the negative IR Raman noncoincidence effect (nNCE).

Initially reported between polarized and depolarized totally symmetric Raman bands of neat liquids, the effect was described by Logan[71] and has been associated with the transition dipole coupling (TDC) mechanism. In 1998, Bertie and Michaelian, however, did not only identify noncoincidence between polarized and depolarized Raman bands, but also found that Raman bands may, quite significantly, differ from the absorption maxima of IR fundamentals.[11] One year later, a thorough computational ab initio MD study of the IR Raman NCE provided evidence that the NCE manifests either with a positive sign (i.e., a blue-shifted IR band when compared to the Raman analog) or with a negative sign, depending on the type of predominant intermolecular interaction forces.[72] In more detail, a later review[12] clearly stated that a positive NCE is observed in liquids structured by strong direction independent dipole−dipole interactions, whereas a negative NCE is found for liquid ensembles that are dominated by hydrogen bonding phenomena.

In our case, the IR Raman NCE was found to be significantly negative (i.e., ∼12 cm^{-1}) for both the symmetric and the asymmetric stretching mode of the As−O bond. Both the sign and the amount of shift are explained by the following three observations, all being in accordance with the theory underlying the IR Raman NCE.[12,72] First, the simulation outcome proved that the solute frequently forms hydrogen bonds with the surrounding solvent. Second, the experiment and the PT2-VSCF evaluation showed that both ν_s (A_1) and ν_{as} (E) are significantly IR active with computationally estimated intensities of 89 and 243 km·mol^{-1}, respectively. Finally, the

dx.doi.org/10.1021/ic4031156 | Inorg. Chem. 2014, 53, 11861−11870

equilibrium dipole moment of H_3AsO_3 was calculated as 2.54 D, implying significant interaction forces with the surrounding solvent.

3.3. Thermodynamic and Kinetic Properties of the Hydrolysis Reactions. Since the occurrence of a chemical reaction is a probabilistic event linked to the respective rate constant, further investigations were carried out to confirm that the PT processes and their time scales are representative. To obtain information regarding the respective chemical equilibria, an acidity estimation has been performed using an established thermodynamic cycle approach as outlined in the literature[73−75] (Figure 7). The resulting expression for the free

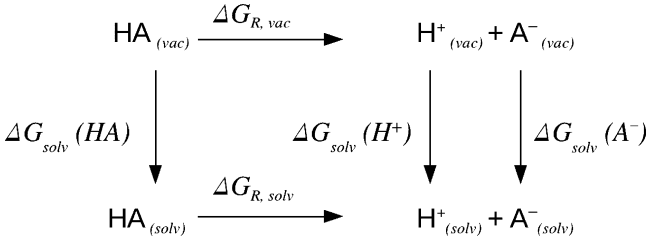

Figure 7. Thermodynamic cycle used for the calculation of pK_a values.[73−75]

energy of reaction for a hydrolysis in solvent $\Delta G_{R,solv}$ is given in eq 1. $G(X)$ corresponds to the free energy of the isolated reactants obtained via the sophisticated high level methods Gaussian-4 (G4)[76] and the complete basis set method CBS-Q//B3.[77,78] The value of −26.3 kJ/mol for $G(H^+)$ is given in literature.[74,75,79] In order to estimate the free energy of solvation ΔG_{solv}, the influence of the surrounding solvent is determined as the difference between vacuum energies and those obtained in implicit solvent using the "Solvation Model Density" (SMD) approach developed by Truhlar and co-workers[80] at the same level of theory. All computations in this context have been carried out with the Gaussian09 package, revision D.01.[81] For $\Delta G_{solv}(H^+)$ the value of −1087 kJ/mol recommended by Hünenberger and Reif[82] has been used. A correction factor of $RT\ln(R'T)$ (7.93 kJ/mol) has to be added to the gas phase energies to account for the different reference states in gas phase (1 atm) and liquid state (1 mol/L).[79,83] The results summarized in Table 3 verify that all arsenic(III)-aquo-complexes observed during the simulation are highly acidic and that these species hydrolyze almost instantaneously in aqueous environment, ultimately leading to $As(OH)_3$.

Additional calculations have been conducted to investigate the kinetic properties of the final hydrolysis step. A reaction path optimization on the MP2 level of theory in implicit solvent (SMD) reevaluating the frequencies in every optimization step and employing the basis sets chosen for the simulation along with an estimation of the rate constant via harmonic transition state theory (eq 2) have been carried out. The intrinsic reaction coordinate has been made available as an *xyz*-file in the Supporting Information. A second value of this rate constant has been derived from conventional transition state calculations (eq 3) on the G4 level of theory using the same implicit solvent model (SMD). For these approaches a model system including additional water molecules stabilizing the educt state is required. When omitting these water molecules, this state does not represent a stable energy minimum and geometry optimizations always lead to the product state $As(OH)_3$. The intrinsic reaction coordinate is depicted in Figure 8a. An interesting feature that can be seen when monitoring the respective donor−hydrogen and acceptor−hydrogen distances (Figure 8b) is that the transition state does not coincide with the actual transfer of the proton. This implies that the rearrangement of the surrounding water molecules has a strong influence on the energetic properties of the reaction coordinate, which agrees well with the conclusions drawn from the simulation. The rate constants derived via harmonic transition state theory k_{hTST} (eq 2) amount to 4.3×10^{12} and 1.3×10^{12} s^{-1} for the forward and the backward reaction, respectively. This corresponds to a pK_a value of −0.5, which is different from the estimation employing the thermodynamic cycle. The second estimation of the rate constant realized via the conventional transition state theory k_{cTST} (eq 3) yielded values of 4.5×10^{12} (forward) and 0.4×10^{12} s^{-1} (backward), which corresponds to a pK_a value of −1.1. The difference to the thermodynamic cycle may be explained by the idealized arrangement of H-bonds not only of the donor and acceptor molecules but also between the acceptor and its surrounding water molecules, which was also observed in the simulation. Only in the case of such an idealized structural arrangement of the two coordinating water molecules, the hydrolysis was observed. Since such an arrangement of water molecules is a prerequisite to investigate the reaction rate via a model system, the resulting rate constants can be assumed to be too large.

Table 3. Results of the Thermodynamic Calculations of the Four Reactants Arising from the Three Hydrolysis Reactions of Aqueous Arsenic(III): Free Energy in a Vacuum Including Electronic, Zero-Point and Thermal Contributions G_{vac} in Ha, Free Electronic Energy in Implicit Solvent G_{solv} in Ha, Free Energy of Solvation ΔG_{solv} in kJ/mol, Free Energy of Reaction in a Vacuum $\Delta G_{R,vac}$ in kJ/mol, Free Energy of Reaction in Implicit Solvent $\Delta G_{R,solv}$ in kJ/mol, and the pK_a Value of the Corresponding Acidic Reactant Obtained at G4 and CBS-Q//B3 Levels of Theory

species	G_{vac}	G_{solv}	ΔG_{solv}	$\Delta G_{R,vac}$	$\Delta G_{R,solv}$	pK_a
			CBS-Q//B3			
$[As(H_2O)_3]^{3+}$	−2462.192066	−2463.084921	−2344.2	−319.4	−142.53	−25.0
$[As(OH)(H_2O)_2]^{2+}$	−2462.303684	−2462.718192	−1088.3	248.5	−96.86	−17.0
$[As(OH)_2(H_2O)]^{1+}$	−2462.199001	−2462.334069	−354.6	763.1	−31.12	−5.5
$As(OH)_3$	−2461.898344	−2461.924908	−69.7			
			G4			
$[As(H_2O)_3]^{3+}$	−2463.169397	−2464.061266	−2341.6	−305.5	−137.62	−24.1
$[As(OH)(H_2O)_2]^{2+}$	−2463.275722	−2463.692670	−1094.7	257.9	−81.86	−14.3
$[As(OH)_2(H_2O)]^{1+}$	−2463.167458	−2463.302835	−355.4	768.5	−22.01	−3.9
$As(OH)_3$	−2462.864729	−2462.890203	−66.9			

dx.doi.org/10.1021/ic4031156 | *Inorg. Chem.* 2014, 53, 11861−11870

Table 4. Results of the Kinetic Calculations of the Last Hydrolysis Reaction of Aqueous Arsenic(III)[a]

species	$\prod_{i=1}^{n}\nu_i$	E_{MP2}	k_{hTST}	G_{G4}	k_{cTST}
educt	6.40×10^{151}	−863.71818623	4.3×10^{12}	−2768.979030	4.5×10^{12}
transition state	3.56×10^{149}	−863.71798738	1.3×10^{12}	−2768.978727	0.4×10^{12}
product	2.94×10^{153}	−863.72294472		−2768.981356	

[a]Columns two to four show data related to the harmonic transition theory approach: product of real wavenumbers in cm^{-n}, electronic energy E_{MP2} in Ha and rate constants for forward and backward reactions k_{hTST} in s^{-1}. The last two columns present data related to the conventional transition theory approach: free energy in implicit solvent including electronic, zero-point and thermal contributions G_{G4}, and rate constants for forward and backward reactions k_{cTST} in s^{-1}.

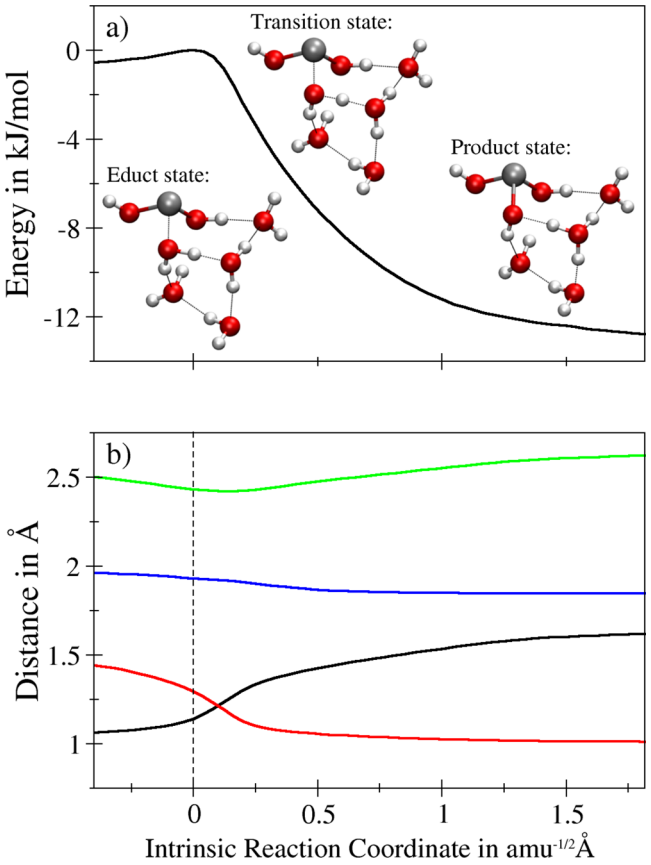

Figure 8. Reaction path for the final hydrolysis step obtained at MP2 level of theory in implicit solvent (SMD) using the depicted model system: (a) potential energy observed along the reaction coordinate as illustrated in the snapshots and (b) selected interatomic distances characterizing the PT event. Coloring corresponds to that used in Figure 2 and S1−3: donor−hydrogen (black), acceptor−hydrogen (red), donor−acceptor (green), arsenic−donor (blue).

Furthermore, since the influence of dynamical recrossings are not taken into account, rate constants determined via transition state theory always mark an upper limit,[84] which may also be a reason for the deviation of the pK_a values determined via the thermodynamic cycle. Nevertheless, the order of magnitude being in the picosecond range clearly confirms that the PT events observed along the simulation trajectory occur on an appropriate time scale, which fully agrees with the expected properties of a highly acidic compound.

$$\Delta G_{R,solv} = G(H^+) + G(A^-) - G(HA) + \Delta G_{solv}(H^+) + \Delta G_{solv}(A^-) - \Delta G_{solv}(HA) + RT\ln(R'T) \quad (1)$$

$$k_{hTST} = \frac{\prod_{i=1}^{n}\nu_i^{min}}{\prod_{i=1}^{n-1}\nu_i^{\ddagger}} e^{-E^{(\ddagger)}-E^{min})/k_BT} \quad (2)$$

$$k_{cTST} = \frac{k_BT}{h} e^{-\Delta G/k_BT} \quad (3)$$

4. CONCLUSION

The dissociative water model developed by Garofalini and Mahadevan was successfully applied in the MM region of a hybrid QMCF-MD simulation for the first time. Monitoring structural and electronic properties revealed a number of interesting details of the hydrolysis process of As^{3+} in aqueous environment. In particular, water molecules adjacent to the hydrolysis center forming H-bonds were found to have a strongly promoting influence on the dissociation. The last hydrolysis stage highlights the importance not only of proper acceptor−proton (i.e., 1.6−1.8 Å) and donor−acceptor distances (i.e., 2.5−2.7 Å), but also H-bond angles close to linearity. In addition, the quantum mechanically derived atomic partial charges gave detailed insight into charge−transfer effects occurring during the three hydrolysis steps. Besides the proton transfer reactions, a study of the final product (i.e., H_3AsO_3) yielded valuable insight, elucidating the structural aspects of the hydrated acid. The conclusions drawn from the simulation agree well with estimations of the chemical equilibria via a thermodynamic cycle approach and the rate constant of the final hydrolysis step via reaction path optimization. The PT2-VSCF approach enabled valuable considerations regarding the performance of the QMCF-MD simulation at the RI-MP2 level of theory. Experimental FT-IR spectra of arsenous acid in acidified, neutral and basic environment were recorded and the data was found to be in very good agreement with the simulation, underlining its quality. Comparing the newly found peak maxima to previously reported Raman data indicated a significant shift in the absorption wavenumbers. The simulation and the PT2-VSCF calculations likewise provided strong evidence of the shift being a result of the IR Raman noncoincidence effect.

■ ASSOCIATED CONTENT

Supporting Information

Figure S1: Selected interatomic distances characterizing the first (Figure S1), second (Figure S2), and third (Figure S3) PT reaction of the hydrolysis of As(III); *xyz* file. This material is available free of charge via the Internet at http://pubs.acs.org.

■ AUTHOR INFORMATION

Corresponding Author

*E-mail: T.Hofer@uibk.ac.at. Tel.: +43-512-507-57102. Fax: +43-512-507-57199.

Notes

The authors declare no competing financial interest.

■ ACKNOWLEDGMENTS

Financial support from a Ph.D. grant of the Leopold-Franzens-University of Innsbruck (Rector Univ. Prof. Dr. Dr. h.c. mult. Tilmann D. Märk) for Lorenz R. Canaval is gratefully acknowledged. This work was supported by the Austrian Ministry of Science BMWF UniInfrastrukturprogramm as part of the Research Focal Point Scientific Computing at the University of Innsbruck.

■ REFERENCES

(1) *Guidelines for Drinking-water Quality*, 3rd ed.; World Health Organization: Geneva, 2008; Vol. *1*.
(2) Cullen, W. R.; Reimer, K. J. *Chem. Rev.* **1989**, *89*, 713−764.
(3) Pokrovski, G.; Gout, R.; Schott, J.; Zotov, A.; Harrichoury, J.-C. *Geochim. Cosmochim. Acta* **1996**, *60*, 737−749.
(4) Maliyekkal, S. M.; Philip, L.; Pradeep, T. *Chem. Eng. J.* **2009**, *153*, 101−107.
(5) Miodragovic, D. U.; Quentzel, J. A.; Kurutz, J. W.; Stern, C. L.; Ahn, R. W.; Kandela, I.; Mazar, A.; O'Halloran, T. V. *Angew. Chem., Int. Ed.* **2013**, *52*, 10749−10752.
(6) Hofer, T. S.; Hitzenberger, M.; Randolf, B. R. *J. Chem. Theory Comput.* **2012**, *8*, 3586−3595.
(7) Mahadevan, T. S.; Garofalini, S. H. *J. Phys. Chem. B* **2007**, *111*, 8919−8927.
(8) Lim, L. H. V.; Bhattacharjee, A.; Randolf, B. R.; Rode, B. M. *Phys. Chem. Chem. Phys.* **2010**, *12*, 12423−12426.
(9) Bhattacharjee, A.; Hofer, T. S.; Pribil, A. B.; Randolf, B. R.; Rode, B. M. *Chem. Phys. Lett.* **2009**, *473*, 176−178.
(10) Bhattacharjee, A.; Hofer, T. S.; Pribil, A. B.; Randolf, B. R.; Rode, B. M. *Phys. Chem. Chem. Phys.* **2010**, *12*, 6244−6246.
(11) Bertie, J. E.; Michaelian, K. H. *J. Chem. Phys.* **1998**, *109*, 6764−6771.
(12) Giorgini, M. G. *Pure Appl. Chem.* **2004**, *76*, 157−169.
(13) Hofer, T.; Pribil, A.; Randolf, B.; Rode, B. *Adv. Quantum Chem.* **2010**, *59*, 213−246.
(14) Weiss, A. K. H.; Hofer, T. S. *RSC Adv.* **2013**, *3*, 1606−1635.
(15) Field, M. J.; Bash, P. A.; Karplus, M. *J. Comput. Chem.* **1990**, *11*, 700−733.
(16) Bakowies, D.; Thiel, W. *J. Phys. Chem.* **1996**, *100*, 10580−10594.
(17) Gao, J. *J. Am. Chem. Soc.* **1993**, *115*, 2930−2935.
(18) Rode, B.; Hofer, T.; Randolf, B.; Schwenk, C.; Xenides, D.; Vchirawongkwin, V. *Theor. Chem. Accounts Theor. Comput. Model. Theor. Chim. Acta* **2006**, *115*, 77−85.
(19) Hofer, T. S.; Randolf, B. R.; Rode, B. M. *Solvation Effects on Molecules and Biomolecules*; Springer: Heidelberg, 2008; Vol. *6*; pp 247−278.
(20) Billeter, S.; van Gunsteren, W. *Comput. Phys. Commun.* **1997**, *107*, 61−91.
(21) Billeter, S.; Van Gunsteren, W. *J. Phys. Chem. A* **1998**, *102*, 4669−4678.
(22) Sagnella, D. E.; Tuckerman, M. E. *J. Chem. Phys.* **1998**, *108*, 2073.
(23) Schmitt, U. W.; Voth, G. A. *J. Phys. Chem. B* **1998**, *102*, 5547−5551.
(24) Vuilleumier, R.; Borgis, D. *J. Chem. Phys.* **1999**, *111*, 4251.
(25) Cuma, M.; Schmitt, U. W.; Voth, G. A. *J. Phys. Chem. A* **2001**, *105*, 2814−2823.
(26) Brancato, G.; Tuckerman, M. E. *J. Chem. Phys.* **2005**, *122*, 224507.
(27) Wu, Y.; Chen, H.; Wang, F.; Paesani, F.; Voth, G. A. *J. Phys. Chem. B* **2008**, *112*, 467−482.
(28) Park, K.; Lin, W.; Paesani, F. *J. Phys. Chem. B* **2011**, *116*, 343−352.
(29) Ufimtsev, I. S.; Kalinichev, A. G.; Martinez, T. J.; Kirkpatrick, R. J. *Phys. Chem. Chem. Phys.* **2009**, *11*, 9420−9430.
(30) Wolf, D.; Keblinski, P.; Phillpot, S. R.; Eggebrecht, J. *J. Chem. Phys.* **1999**, *110*, 8254−8282.
(31) Marx, D. *ChemPhysChem* **2006**, *7*, 1848−1870.
(32) Sagnella, D. E.; Tuckerman, M. E. *J. Chem. Phys.* **1998**, *108*, 2073−2083.
(33) Tuckerman, M. E.; Marx, D.; Klein, M. L.; Parrinello, M. *Science* **1997**, *275*, 817−820.
(34) Marx, D.; Tuckerman, M. E.; Hutter, J.; Parrinello, M. *Nature* **1999**, *397*, 601−604.
(35) Bowman, J. M. *J. Chem. Phys.* **1978**, *68*, 608−610.
(36) Bowman, J. M. *Acc. Chem. Res.* **1986**, *19*, 202−208.
(37) Carter, S.; Culik, S. J.; Bowman, J. M. *J. Chem. Phys.* **1997**, *107*, 10458−10469.
(38) Chaban, G. M.; Jung, J. O.; Gerber, R. B. *J. Chem. Phys.* **1999**, *111*, 1823−1829.
(39) Yagi, K.; Taketsugu, T.; Hirao, K.; Gordon, M. S. *J. Chem. Phys.* **2000**, *113*, 1005−1017.
(40) Jung, J. O.; Gerber, R. B. *J. Chem. Phys.* **1996**, *105*, 10332−10348.
(41) Norris, L. S.; Ratner, M. A.; Roitberg, A. E.; Gerber, R. B. *J. Chem. Phys.* **1996**, *105*, 11261−11267.
(42) Pele, L.; Gerber, R. B. *J. Chem. Phys.* **2008**, *128*, 165105.
(43) Schmidt, M. W.; Baldridge, K. K.; Boatz, J. A.; Elbert, S. T.; Gordon, M. S.; Jensen, J. H.; Koseki, S.; Matsunaga, N.; Nguyen, K. A.; Su, S.; Windus, T. L.; Dupuis, M.; Montgomery, J. A. *J. Comput. Chem.* **1993**, *14*, 1347−1363.
(44) Tomasi, J.; Mennucci, B.; Cammi, R. *Chem. Rev.* **2005**, *105*, 2999−3094.
(45) Dunning, T. H. *J. Chem. Phys.* **1989**, *90*, 1007−1023.
(46) Peterson, K. A. *J. Chem. Phys.* **2003**, *119*, 11099−11112.
(47) Hehre, W. J.; Ditchfield, R.; Pople, J. A. *J. Chem. Phys.* **1972**, *56*, 2257−2261.
(48) Berendsen, H. J. C.; Postma, J. P. M.; van Gunsteren, W. F.; DiNola, A.; Haak, J. R. *J. Chem. Phys.* **1984**, *81*, 3684−3690.
(49) Mulliken, R. S. *J. Chem. Phys.* **1955**, *23*, 1833−1840.
(50) Mulliken, R. S. *J. Chem. Phys.* **1955**, *23*, 1841−1846.
(51) *TURBOMOLE*, V6.3 2011, a Development of University of Karlsruhe and Forschungszentrum Karlsruhe GmbH, 1989−2007, TURBOMOLE GmbH, since 2007; http://www.turbomole.com.
(52) Ahlrichs, R.; Bär, M.; Häser, M.; Horn, H.; Kölmel, C. *Chem. Phys. Lett.* **1989**, *162*, 165−169.
(53) Häser, M.; Ahlrichs, R. *J. Comput. Chem.* **1989**, *10*, 104−111.
(54) Weigend, F.; Häser, M. *Theor. Chem. Acc.* **1997**, *97*, 331−340.
(55) Hättig, C.; Hellweg, A.; Köhn, A. *Phys. Chem. Chem. Phys.* **2006**, *8*, 1159−1169.
(56) Weigend, F.; Häser, M.; Patzelt, H.; Ahlrichs, R. *Chem. Phys. Lett.* **1998**, *294*, 143−152.
(57) Humphrey, W.; Dalke, A.; Schulten, K. *J. Mol. Graph.* **1996**, *14*, 33−38.
(58) Loehr, T. M.; Plane, R. A. *Inorg. Chem.* **1968**, *7*, 1708−1714.
(59) Norton, R. H.; Beer, R. *J. Opt. Soc. Am.* **1976**, *66*, 259−264.
(60) Ramírez-Solís, A.; Mukopadhyay, R.; Rosen, B. P.; Stemmler, T. L. *Inorg. Chem.* **2004**, *43*, 2954−2959.
(61) Lockwood, G. K.; Garofalini, S. H. *J. Phys. Chem. B* **2013**, *117*, 4089−4097.
(62) Tuckerman, M. E.; Marx, D.; Parrinello, M. *Nature* **2002**, *417*, 925−929.
(63) Berkelbach, T. C.; Lee, H.-S.; Tuckerman, M. E. *Phys. Rev. Lett.* **2009**, *103*, 238302.
(64) Coskuner, O.; Allison, T. C. *ChemPhysChem* **2009**, *10*, 1187−1189.
(65) Rycroft, C. H. *Chaos* **2009**, *19*, 041111.
(66) Poupon, A. *Curr. Opin. Struct. Biol.* **2004**, *14*, 233−241.
(67) Voronoi, G. *J. Reine Angew. Math.* **1908**, *133*, 97178.
(68) Shannon, R. *Acta Crystallogr., Sect. A* **1976**, *32*, 751−767.
(69) Mantina, M.; Chamberlin, A. C.; Valero, R.; Cramer, C. J.; Truhlar, D. G. *J. Phys. Chem. A* **2009**, *113*, 5806−5812.
(70) Wood, S. A.; Tait, C. D.; Janecky, D. R. *Geochem. Trans.* **2002**, *3*, 31.

(71) Logan, D. E. *Chem. Phys.* **1986**, *103*, 215−225.
(72) Torii, H. *J. Phys. Chem. A* **1999**, *103*, 2843−2850.
(73) da Silva, C. O.; da Silva, E. C.; Nascimento, M. A. C. *J. Phys. Chem. A* **1999**, *103*, 11194−11199.
(74) Jang, Y. H.; Sowers, L. C.; Çağin, T.; Goddard, W. A. *J. Phys. Chem. A* **2001**, *105*, 274−280.
(75) Topol, I.; Tawa, G.; Burt, S.; Rashin, A. *J. Phys. Chem. A* **1997**, *101*, 10075−10081.
(76) Curtiss, L. A.; Redfern, P. C.; Raghavachari, K. *J. Chem. Phys.* **2007**, *126*, 084108.
(77) Montgomery, J. A., Jr; Frisch, M. J.; Ochterski, J. W.; Petersson, G. A. *J. Chem. Phys.* **1999**, *110*, 2822−2827.
(78) Montgomery, J. A., Jr; Frisch, M. J.; Ochterski, J. W.; Petersson, G. A. *J. Chem. Phys.* **2000**, *112*, 6532−6542.
(79) Liptak, M. D.; Shields, G. C. *J. Am. Chem. Soc.* **2001**, *123*, 7314−7319.
(80) Marenich, A. V.; Cramer, C. J.; Truhlar, D. G. *J. Phys. Chem. B* **2009**, *113*, 6378−6396.
(81) Frisch, M. J.; Trucks, G. W.; Schlegel, H. B.; Scuseria, G. E.; Robb, M. A.; Cheeseman, J. R.; Scalmani, G.; Barone, V.; Mennucci, B.; Petersson, G. A.; et al. *Gaussian 09*, Revision D.01; Gaussian Inc.: Wallingford CT, 2009.
(82) Hünenberger, P.; Reif, M. *Single-Ion Solvation: Experimental and Theoretical Approaches to Elusive Thermodynamic Quantities*; RSC Theoretical and Computational Chemistry Series; Royal Society of Chemistry: Cambridge, 2011.
(83) Namazian, M.; Zakery, M.; Noorbala, M. R.; Coote, M. L. *Chem. Phys. Lett.* **2008**, *451*, 163−168.
(84) Wales, D. *Energy Landscapes: Applications to Clusters, Biomolecules and Glasses*; Cambridge Molecular Science; Cambridge University Press: Cambridge, 2003.